Constrained density functional for noncollinear magnetism

Pui-Wai Ma* and S. L. Dudarev
CCFE, Culham Science Centre, Abingdon, Oxfordshire OX14 3DB, United Kingdom
(Received 4 September 2014; revised manuscript received 22 December 2014; published 24 February 2015)

Energies of arbitrary small- and large-angle noncollinear excited magnetic configurations are computed using a highly accurate constrained density functional theory approach. Numerical convergence and accuracy are controlled by the choice of Lagrange multipliers λ_I entering the constraining conditions. The penalty part E_p of the constrained energy functional at its minimum is shown to be inversely proportional to λ_I, enabling a simple, robust, and accurate iterative procedure to be followed to find a convergent solution. The method is implemented as a part of *ab initio* VASP package, and applied to the investigation of noncollinear B2-like and ⟨001⟩ double-layer antiferromagnetic configurations of bcc iron, Fe_2 dimer, and amorphous iron. Forces acting on atoms depend on the orientations of magnetic moments, and the proposed approach enables constrained self-consistent noncollinear magnetic and structural relaxation of large atomic systems to be carried out.

DOI: 10.1103/PhysRevB.91.054420 PACS number(s): 71.15.−m, 75.50.Xx, 75.50.Kj

I. INTRODUCTION

Many materials have noncollinear magnetic ground states, including geometrically frustrated magnets [1–3], spin glasses [4–6] or spin spirals that form, for example, in face-centered cubic Fe [7–13]. Excited magnetic states are almost always noncollinear [14–16]. For example, ferromagnetic metals often have collinear magnetic ground states but at elevated temperatures magnetic moment vectors are noncollinear and disordered. If temperature exceeds the Curie temperature of the material, magnetic long-range order vanishes, and the material undergoes a transition into a paramagnetic state [17–19].

Although *ab initio* calculations often assume collinear magnetic configurations, spin-polarized density functional theory (DFT) [20] does not impose any constraints on the directions of atomic magnetic moments. Theoretical foundations of unconstrained noncollinear DFT are well established [2,3,8,11,21–28] and are widely adopted in *ab initio* programs [29–31].

Magnetic DFT calculations are often performed in the atomic sphere approximation [3,8,11,21,22,28] (ASA) where the local spin quantization axis (SQA) is associated with a sphere centered at a particular atom. Noncollinear magnetism in the ASA is an interatomic phenomenon, where magnetic moments of neighboring atomic spheres have different orientations. On the other hand, spin density matrix is a continuous spatially varying field [23–27] enabling the treatment of both *inter*- and *intra*atomic noncollinear magnetism. Spin density matrix-based methods also have the advantage that atomic and magnetic relaxations can be performed simultaneously and self-consistently.

Magnetic excitations influence the stability of phases, defect structures, and elastic constants in magnetic iron-based alloys [32–46]. They also affect self-diffusion in magnetic materials, especially near the Curie temperature [47,48]. Within the DFT framework, the effect of magnetic excitations on atomic positions can be investigated by requiring that atoms adopt a particular magnetic configuration, and compare forces acting on atoms assuming different magnetic structures; *ab initio* spin dynamics simulations [49–52] can be performed through a series of magnetic configurations generated in a sequential order [53,54].

A noncollinear magnetic configuration does not in general correspond to an energy minimum. Still it can be investigated using a minimization principle by imposing constraints on magnetic moments [27,28,53–57]. A scheme [57] that requires fixing the direction of a local SQA works only in the limit of small canting [28]. A more reliable way of generating noncollinear configurations involves using Lagrange multipliers [27,28,53–56]. A set of Lagrange multipliers and a penalty term in the total energy functional are introduced, resulting in a penalty potential in the Kohn-Sham equations. This nudges the (local) charges and (local) magnetic moments towards a particular desired configuration. Using the method, interatomic exchange parameters [57–59] can be elucidated, for example, by comparing energies of collinear and spin spiral configurations.

There are several constrained DFT algorithms for generating noncollinear magnetic configurations. They use different penalty energy terms. In some cases [27,28,53–55], vector fields are used as Lagrange multipliers, requiring a separate procedure for computing the fields at each iteration step. In VASP [31], two constrained methods are implemented, both involving scalar Lagrange multipliers. One of the methods is invariant with respect to the reversal of local magnetic moments, resulting in degenerate energy minima. The other method constrains all the components of magnetic moment vectors, and not just their directions.

None of the above approaches guarantees that the penalty energy and penalty potential vanish for a chosen set of Lagrange multipliers, whereas controlling accuracy is crucial to an application of a constrained method. In what follows, we describe a method that guarantees accuracy through a suitable choice of control parameters. The convergence conditions are established and proven analytically. In Sec. II, we describe the method and show that the penalty energy term at the minimum of the constrained energy functional is inversely proportional to the magnitude of Lagrange multipliers. In Sec. III, we discuss numerical convergence. Section IV describes applications of the method to several atomic and magnetic structures of iron. They are (i) B2-like and double-layer antiferromagnetic configurations realized on

*Leo.Ma@ccfe.ac.uk

bcc lattice, (ii) a Fe_2 dimer with atomic magnetic moment vectors pointing in prescribed directions, and (iii) amorphous iron with random directions of magnetic moments.

II. THEORY

Hobbs *et al.* [25] proposed an algorithm for computing unconstrained noncollinear magnetic configurations and implemented it in VASP (Vienna *ab initio* simulation package) [31], using a projector augmented-wave (PAW) method [60]. In our work, we follow a similar methodology.

The advantage of the Hobbs *et al.* [25] method is that it assumes no pre-defined SQA and enables relaxation of both atomic and magnetic degrees of freedom. However, it contains an element of ambiguity associated with the definition of local atomic magnetic moments. Local magnetic moments vary as functions of integration volumes, and their values depend on the choice of the Wigner-Seitz cell or the radius of the corresponding atomic sphere.

For example, the magnetic moment of an atom can be defined as

$$\mathbf{M}_I = \int_{\Omega_I} \mathbf{m}(\mathbf{r}) d^3 r, \tag{1}$$

where $\mathbf{m}(\mathbf{r})$ is a spatially varying magnetization density vector, and Ω_I is a sphere centered at atom I.

In what follows, instead of using $\mathbf{M}_I$ directly, we use an alternative definition of magnetic moment, namely

$$\mathbf{M}_I^F = \int_{\Omega_I} \mathbf{m}(\mathbf{r}) F_I(|\mathbf{r} - \mathbf{r}_I|) d^3 r, \tag{2}$$

where $F_I(|\mathbf{r} - \mathbf{r}_I|) = \sin(x)/x$ and $x = \pi(|\mathbf{r} - \mathbf{r}_I|)/R_I$. F_I decreases monotonically to zero towards the boundary of the atomic sphere. A similar definition of $\mathbf{M}_I^F$ was adopted in VASP in relation to other constrained methods.

The integration volume involved in a calculation of a local magnetic moments can be defined in various ways. For example, we may adopt the Bader charge analysis [61,62]. It divides atoms by zero flux surfaces, which are the surfaces corresponding to minimum charge density. An alternative approach would be to equate the integration volume to the volume of the Wigner-Seitz cell. However, these methods require using the functional form of F_I more complicated than the current one, which depends only on a single parameter R_I.

The constrained total energy functional now has the form,

$$E = E_0 + E_p \tag{3}$$

$$= E_0 + \sum_I \lambda_I \left(\left|\mathbf{M}_I^F\right| - \mathbf{e}_I \cdot \mathbf{M}_I^F \right), \tag{4}$$

where E_0 is the DFT energy of the material, E_p is the penalty energy term, $\mathbf{e}_I$ is a unit vector in the desired direction of the local magnetic moment, and λ_I is a Lagrange multiplier associated with site I. The dimensionality of λ_I is the same as of external magnetic field.

The penalty energy term in (4) introduces an effective extra potential inside each sphere Ω_I centered at atom I, which is given by

$$V_I(\mathbf{r}) = -\mathbf{b}_p(\mathbf{r}) \cdot \boldsymbol{\sigma}, \tag{5}$$

where $\boldsymbol{\sigma}$ is the vector of Pauli matrices, and

$$\mathbf{b}_p(\mathbf{r}) = -\frac{\delta E_p}{\delta \mathbf{m}(\mathbf{r})} \tag{6}$$

$$= -\lambda_I \left(\frac{\mathbf{M}_I^F}{\left|\mathbf{M}_I^F\right|} - \mathbf{e}_I \right) F_I(|\mathbf{r} - \mathbf{r}_I|) \tag{7}$$

is an additional penalty "field" in the Kohn-Sham equations. Equations (4) and (7) show that both E_p and $V_I(\mathbf{r})$ terms vanish only if vector $\mathbf{M}_I^F$ points in the same direction as $\mathbf{e}_I$.

From Eq. (6) we find that function $F_I(|\mathbf{r} - \mathbf{r}_I|)$ eliminates the discontinuity of the effective potential at the boundary of atomic sphere Ω_I. Separating the core and interstitial regions, like in the approach by Kurz *et al.* [27] or in the ASA, is not necessary. The part played by the penalty term appears similar to the action of the local spatially varying external magnetic field.

We now prove that in the limit $\lambda_I \to \infty$, $E_p \to 0$ and is inversely proportional to λ_I. We rewrite the constrained total energy (4) as

$$E = E_0 + \sum_I \lambda_I \left|\mathbf{M}_I^F\right| (1 - \cos\theta_I), \tag{8}$$

where θ_I is the angle between $\mathbf{M}_I^F$ and $\mathbf{e}_I$. At an extremum of the energy functional the first derivative of the total energy with respect to θ_I must vanish, namely

$$0 = \left.\frac{\delta E}{\delta \theta}\right|_{\theta_I} = \left.\frac{\delta E_0}{\delta \theta}\right|_{\theta_I} + \lambda_I \left|\mathbf{M}_I^F\right| \sin\theta_I. \tag{9}$$

From this equation it follows that

$$\sin\theta_I = -\frac{1}{\lambda_I \left|\mathbf{M}_I^F\right|} \left.\frac{\delta E_0}{\delta \theta}\right|_{\theta_I}. \tag{10}$$

If θ_I is small, we approximate the left-hand side by $\sin\theta_I \approx \theta_I + O(\theta_I^3)$, and extend the Taylor expansion to the first order in the right-hand side of the equation, namely

$$\theta_I = -\frac{1}{\lambda_I \left|\mathbf{M}_I^F\right|} \left(\left.\frac{\delta E_0}{\delta \theta}\right|_0 + \left.\frac{\delta^2 E_0}{\delta \theta^2}\right|_0 \theta_I \right). \tag{11}$$

We now introduce notations $K_1 = \delta E_0/\delta\theta|_0$ and $K_2 = \delta^2 E_0/\delta\theta^2|_0$. These quantities are the first and second derivatives of energy with respect to θ at $\theta = 0$. K_1 and K_2 do not depend on θ_I, and we can write

$$\theta_I = -\frac{K_1}{\lambda_I \left|\mathbf{M}_I^F\right| + K_2}. \tag{12}$$

Similarly, if θ_I is small, we approximate the penalty energy E_p as $(1 - \cos\theta_I) \approx \theta_I^2/2 + O(\theta_I^4)$,

$$E_p \approx \sum_I \lambda_I \left|\mathbf{M}_I^F\right| \frac{\theta_I^2}{2}. \tag{13}$$

Inserting Eq. (12) into Eq. (13), we arrive at

$$E_p = \frac{1}{2} \sum_I \lambda_I \left|\mathbf{M}_I^F\right| \left(\frac{K_1}{\lambda_I \left|\mathbf{M}_I^F\right| + K_2} \right)^2. \tag{14}$$

From the above analysis we conclude that in the limit where λ_I is large,

$$E_p \propto 1/\lambda_I. \tag{15}$$

This proves that $E_p \to 0$ if $\lambda_I \to \infty$.

Our method is not constrained by either the geometry of the system or the choice of magnetic structure, since functional (4) can be computed for any system described by a spin density matrix. The direction of $\mathbf{M}_I$ may not be exactly the same as $\mathbf{M}_I^F$, due to intraatomic noncollinearity, but they are fairly close if electrons are well localized, which is indeed the case for d and f electrons. We discuss this in detail in the context of applications of the method described below.

III. NUMERICAL CONVERGENCE

In this section, we first examine numerical convergence and the choice of Lagrange multipliers λ_I. Then, we discuss the choice of radius R_I in Eq. (1) above. In the analysis given below, if the values of λ and R are not referred to a particular atom, they are assumed to apply to all the atoms in the simulation cell.

A. Choice of λ_I

A B2-like magnetic configuration can be constructed in bcc Fe using a cubic unit cell with two atoms, where the orientation of the magnetic moment of the central atom is different from the orientation of the magnetic moment of the atom in the corner of the cell. Figure 1 shows a magnetic structure where the angle between the two magnetic moments is 90°. Our calculations are performed in generalized gradient approximation (GGA) using the Perdew-Burke-Ernzerhof (PBE) [63] exchange-correlation functional, which is known to predict the correct bcc ferromagnetic ground state [36]. We include relativistic corrections, but neglect spin-orbit coupling. We use a pseudopotential with 14 valence electrons and a $24 \times 24 \times 24$ k-point mesh. Energy cutoff for plane wave expansion is set at 400 eV, periodic boundary conditions are applied, and the lattice constant is assumed to be 2.83 Å, which is the GGA-PBE equilibrium lattice constant. The results agree well with literature data [36,64].

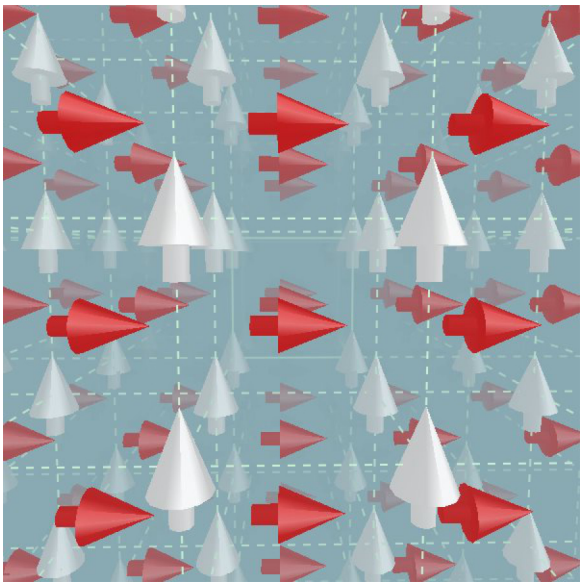

FIG. 1. (Color online) A realization of B2-like magnetic configuration in bcc iron. The angle between magnetic moments of atoms forming the two magnetic sublattices is 90°.

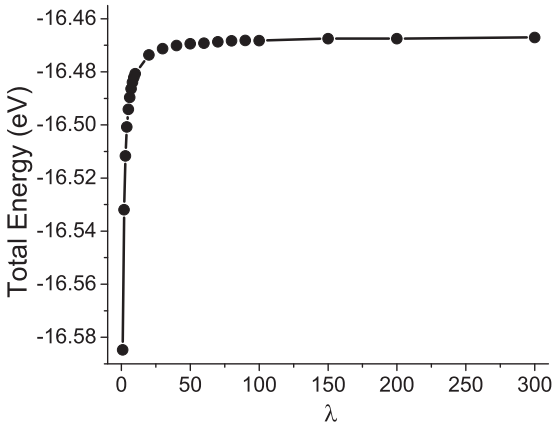

FIG. 2. Total energy E of a bcc Fe unit cell with two atoms per cell, corresponding to the magnetic configuration shown in Fig. 1. Parameter λ varies from 1 to 300.

Figure 2 shows the total energy E of a unit cell as a function of λ, where λ varies in the interval from 1 to 300. In the limit of large λ, the total energy asymptotically approaches a constant value. Figure 3 shows that the penalty energy E_p is inversely proportional to λ, in agreement with Eqs. (14) and (15). At $\lambda = 200$ the value of E_p does not exceed 1×10^{-3} eV. This shows that the convergence of the method with respect to the total energy can be improved by simply increasing the magnitude of Lagrange multipliers λ_I. Since Lagrange multipliers are input parameters, they do not require tuning during the self-consistent iteration procedure. A moderate value of λ should be used initially, to avoid causing numerical instabilities in the iterative procedure due to the large initial value of the penalty potential [Eqs. (5)–(7)]. This does not present a problem in applications, since the value of λ can be adjusted during the search for a minimum.

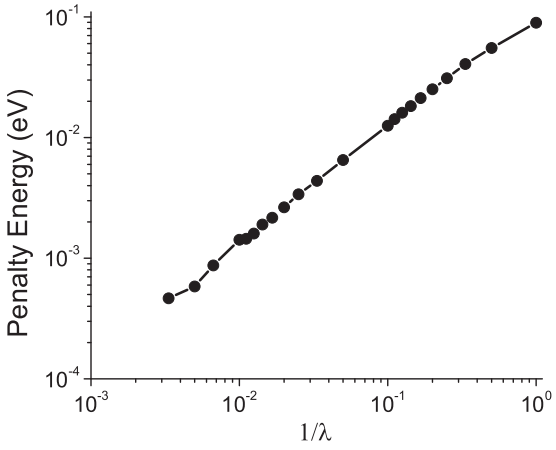

FIG. 3. Penalty energy E_p of a bcc Fe unit cell containing two atoms per cell, corresponding to the magnetic configuration shown in Fig. 1. Parameter λ varies from 1 to 300. In accord with Eqs. (14) and (15), E_p is inversely proportional to λ.

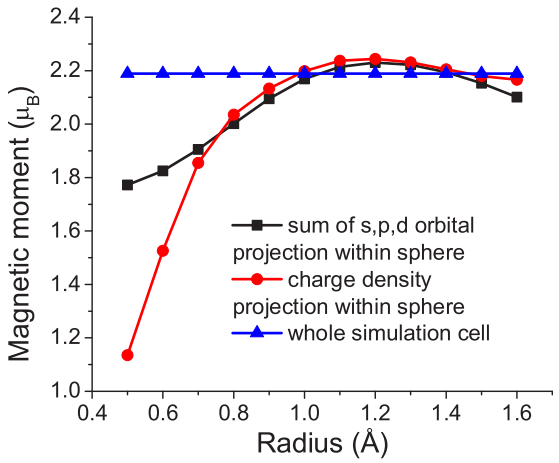

FIG. 4. (Color online) The magnitude of atomic magnetic moment of Fe in ferromagnetic bcc structure. The moment is evaluated as (i) a sum of projections onto s, p, d orbitals within a sphere of a given radius R_I, or (ii) a projection of the total magnetization density onto a sphere of radius R_I, and (iii) an integral of the magnetization density over the entire unit cell. For $R_I = 1.393$ Å, Ω_I equals the volume of the unit cell.

B. Choice of R_I

Since the magnetic moment density $\mathbf{m}(\mathbf{r})$ is a spatially varying quantity, the magnitude of $\mathbf{M}_I$ depends on the choice of radius R_I of sphere Ω_I. Figure 4 shows how atomic magnetic moment $|\mathbf{M}_I|$ of ferromagnetic bcc Fe varies as a function of R_I. A primitive unit cell is used for this calculation, and the moment is evaluated as (i) a sum of projections onto s, p, and d orbitals within a sphere of radius R_I, (ii) a projection of the total charge density within a sphere of particular radius R_I, and (iii) an integral of the total magnetization density over the entire unit cell. For $R = 1.393$ Å, Ω equals the volume of the unit cell. Similarly, in Fig. 5, we show average values of $|\mathbf{M}_I|$ calculated as a sum of orbital projection and magnetization density projection onto a sphere in an antiferromagnetic Fe bcc structure, where the unit cell contains two atoms.

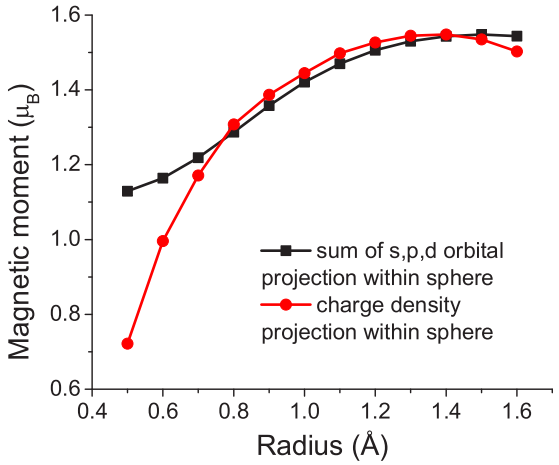

FIG. 5. (Color online) Magnitude of atomic magnetic moment in antiferromagnetic bcc structure of Fe computed using a two-atom cubic unit cell. The moment is calculated as (i) a sum of projections onto s, p, d orbitals within a sphere of radius R_I, (ii) a projection of the total magnetization density onto a sphere of radius R_I. The total magnetic moment of the cell is zero.

Both figures show that $|\mathbf{M}_I|$ increases as a function of R, and is maximum at 1.2 Å in Fig. 4, and 1.3 Å in Fig. 5. There is no unambiguously defined asymptotic value of magnetic moment. From Fig. 4 we can define the magnetic moment of a single Fe atom as $2.2\mu_B$ by integrating the magnetization density over the entire unit cell. However, this definition does not apply to antiferromagnetic configurations since the total magnetic moment of a cell is zero. Choosing R is only necessary when calculating $\mathbf{M}_I$ or E_p, since in the limit of large λ this parameter does not affect the computed values of DFT energy E_0, or the forces acting on atoms. Using the data shown in Figs. 4 and 5, we choose R in the range from 1.0 to 1.6 Å.

IV. APPLICATIONS

In what follows we apply the method described above to several noncollinear atomic magnetic configurations. First, we explore B2-like and ⟨100⟩ double layer antiferromagnetic configurations in bcc iron. Then we analyze a simple magnetic molecule, a Fe_2 dimer. Finally, we apply our method to the magnetic structure of amorphous Fe. Unless stated otherwise, all the calculations described below were performed for $\lambda = 200$.

A. BCC Fe: B2-like and ⟨100⟩ double layer antiferromagnetic configurations

A B2-like magnetic configuration on the bcc lattice (cf. Fig. 1) can also be realized for an arbitrary angle between magnetic moments of atoms forming the two sublattices. Figure 6 shows the magnitude of magnetic moment vectors $|\mathbf{M}_I|$ of both atoms, and the energy E of a unit cell as a function of angle between the moments, assuming that the moment vectors are co-planar. Vectors $\mathbf{M}_I$ are calculated as projections of the total magnetization density onto spheres Ω, where the volume of the spheres equals the volume of an atom. We see that $|\mathbf{M}_I| = 2.22\mu_B$ in the ferromagnetic state and $|\mathbf{M}_I| = 1.52\mu_B$ in the antiferromagnetic state. The difference between the energies of antiferromagnetic and ferromagnetic configurations is 0.45 eV per atom.

Similarly, Herper *et al.* [36] found, using WIEN95 code and full-potential linearized augmented plane-wave (FLAPW) calculations, that the atomic magnetic moment in the ferromagnetic state is $2.17\mu_B$ and in the antiferromagnetic state it is $1.25\mu_B$. The difference between the energies of the two states is 0.44 eV per atom. Soulairol *et al.* [37] also found 0.44 eV per atom energy difference using the PWSCF code and the PAW method. They found that the atomic magnetic moment varied from $2.19\mu_B$ to $2.25\mu_B$ in the ferromagnetic state, and from $1.3\mu_B$ to $1.9\mu_B$ in the antiferromagnetic state, depending on DFT approximations used in the calculations. Recently, Wróbel *et al.* [65] used an unconstrained collinear method in VASP and found that the energy difference between FM and AFM configurations was 0.444 eV per atom, whereas the magnitude of atomic magnetic moments was $|\mathbf{M}_I| = 2.199\mu_B$ in the ferromagnetic and $|\mathbf{M}_I| = 1.290\mu_B$ in the antiferromagnetic states.

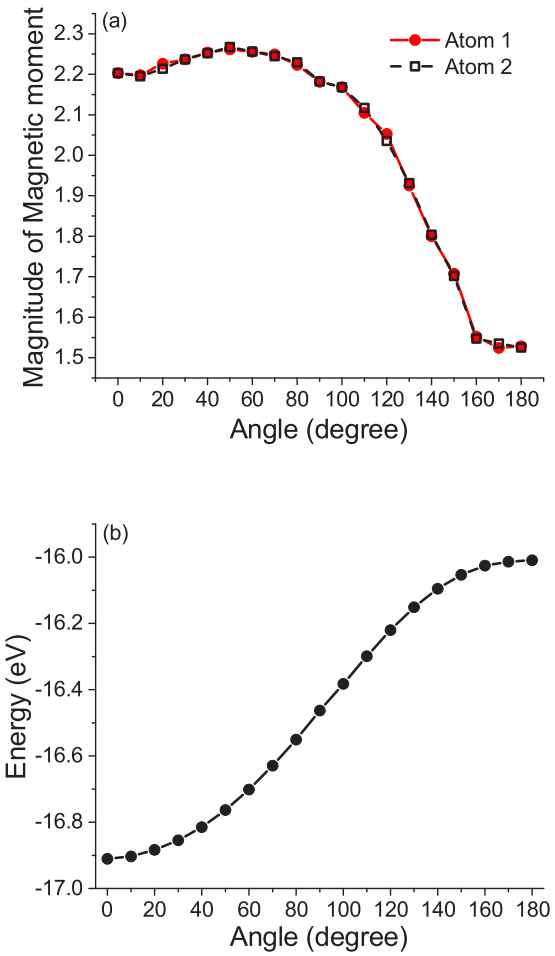

FIG. 6. (Color online) (a) Magnitudes of magnetic moments and (b) the total energy of a cell shown as a function of the angle between magnetic moments of the two atoms forming a B2-like magnetic structure similar to that shown in Fig. 1. Calculations were performed for the bcc lattice constant of 2.83 Å.

Kurz *et al.* [27] used a constrained method with FLAPW to investigate the above magnetic structures. Variation of energy and magnetic moment as functions of the angle between the moments were very similar to our results. The atomic magnetic moment was found to be $2.1\mu_B$ in the ferromagnetic and $1\mu_B$ in the antiferromagnetic states, and the energy difference was 0.35 eV per atom. Our analysis shows that the magnitude of atomic magnetic moments $|\mathbf{M}_I|$ is maximum when the angle between the moments is close to 50°.

We now consider a ⟨100⟩ double layer antiferromagnetic (DLAFM) configuration of bcc Fe. We use this example to perform self-consistent relaxation of both magnetic moments and atomic positions using the constrained method described above. We also investigate the effect of magnetic excitations on atomic configurations. Such analysis cannot be performed using any other means but a constrained density functional. Indeed, since DLAFM is a metastable magnetic state, conventional magnetic relaxations would drive the system towards ferromagnetic ground state regardless of the choice of the initial magnetic configuration.

A unit cell now contains four atoms, and we use a $24 \times 24 \times 12$ k-point mesh. The c/a aspect ratio of the simulation cell is kept fixed to ensure that changes in atomic positions do not interfere with magnetic relaxation. Figure 7(a) shows the directions of magnetic moments in the unrelaxed DLAFM configuration computed for the lattice constant of 2.83 Å. Magnetic moments are calculated as projections of the total magnetization density onto spheres with radii $R_I = 1.0$ Å. Figure 7(b) shows directions of forces induced as a result of the imposed magnetic order. The magnitude of forces is close to 0.25 eV/Å.

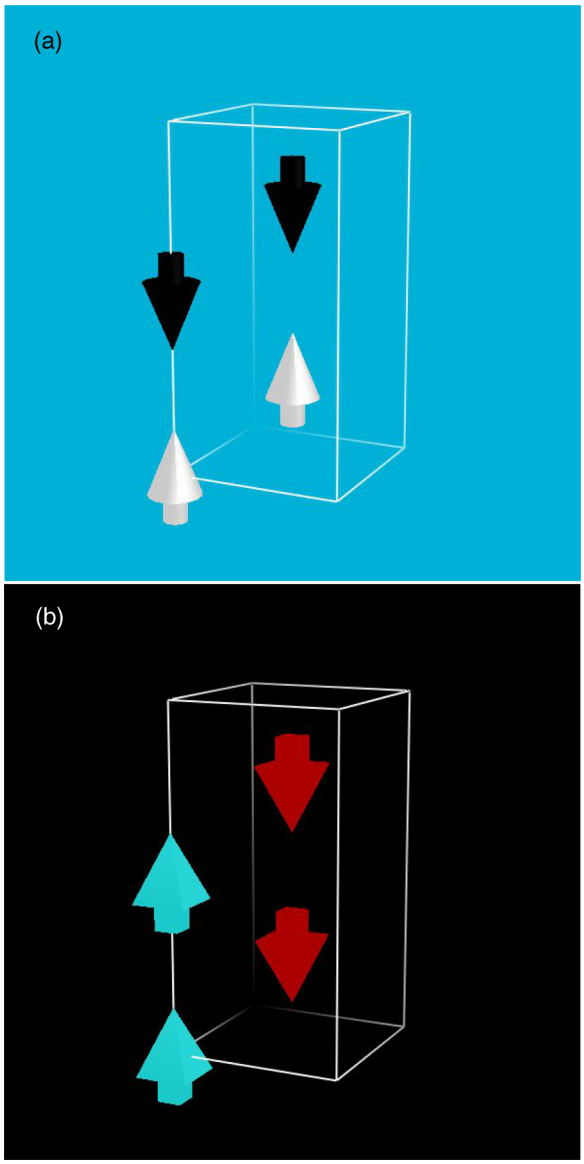

FIG. 7. (Color online) ⟨100⟩ double layer antiferromagnetic (DLAFM) configuration of bcc iron, before ionic relaxation. The lattice constant is 2.83 Å. (a) Directions of magnetic moments. The magnitude of each magnetic moment is $2.08\mu_B$. (b) Forces induced in the structure by the imposed magnetic order. The magnitude of force on each atom is 0.25 eV/Å. Forces are attractive (repulsive) if the magnetic moments of atoms in the two adjacent layers are parallel (antiparallel).

Figure 8 shows the energy and magnetic moment per atom in the DLAFM configuration computed for relaxed and unrelaxed atomic structures. Energy per atom in the

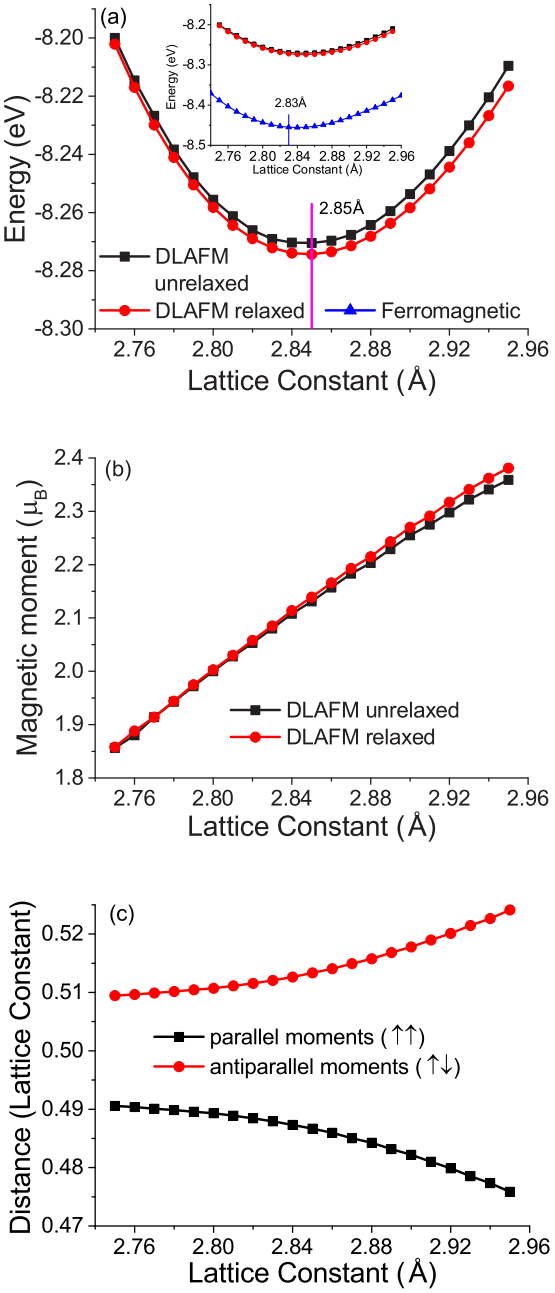

FIG. 8. (Color online) (a) Energy per atom plotted as a function of lattice constant for relaxed and unrelaxed ⟨100⟩ double layer antiferromagnetic and ferromagnetic configurations realized on bcc lattice. (b) Magnitude of atomic magnetic moments plotted as a function of lattice constant for relaxed and unrelaxed configurations. (c) Distance between atomic layers in the ⟨100⟩ direction in relaxed atomic configurations computed for the parallel and antiparallel orientations of magnetic moments.

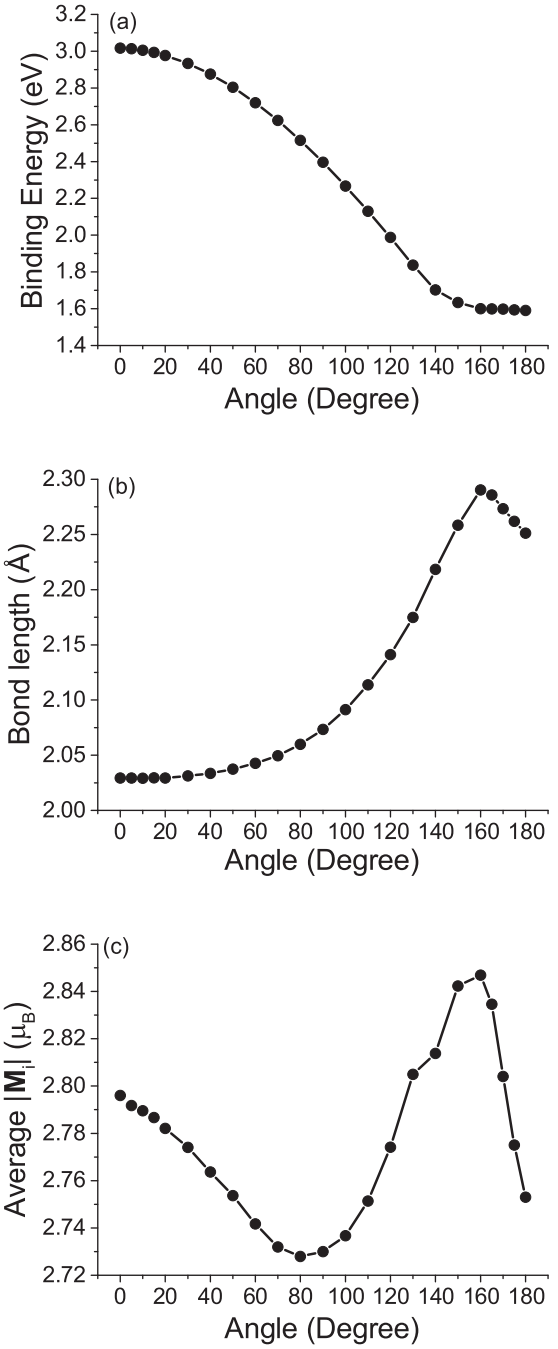

FIG. 9. (a) Binding energy E_B, (b) relaxed bond length R_b, and (c) average magnitude of atomic magnetic moment $|\mathbf{M}_I|$ in a Fe_2 dimer. All the values are plotted as functions of the angle between magnetic moments of the two atoms forming the dimer.

ferromagnetic state, also computed as a function of the lattice constant, is shown for comparison. Figure 8 also shows the distance between magnetically ordered relaxed atomic layers.

The difference between the energies of relaxed and unrelaxed configurations is relatively small, for example, for the equilibrium lattice constant of 2.85 Å it is approximately 0.015 eV/atom. Magnetic moments of relaxed and unrelaxed configurations differ by only a small amount, too. Our results are in agreement with those by Wróbel *et al.* [65], who carried out calculations in the collinear approximation, finding the equilibrium volume of 11.34 Å^3/atom, $|\mathbf{M}_I| = 2.104\mu_B$ and the energy difference between the DLAFM and ferromagnetic configurations of 0.163 eV/atom.

At the same time, by examining the relaxed configurations, we find non-negligible variation of spacing between the atomic layers. Atomic layers with parallel orientations of magnetic

moments relax towards each other. Separation between the layers decreases from exactly half of lattice constant a to $0.49a$, for $a = 2.76$ Å. The two layers move even closer to $0.475a$ if $a = 2.95$ Å. On the other hand, if magnetic moments of the adjacent layers are antiparallel, the interlayers spacing increases accordingly.

The above example illustrates the significance of taking into account directions of local magnetic moments in the context of discussion of forces acting on atoms. It also shows that magnetic excitations induce additional interatomic forces and modify the geometry of atomic configurations. Our conclusions agree with the recent analysis by Körmann *et al.* [18,19] who find the occurrence of strong phonon-magnon coupling in iron at high temperatures. Körmann *et al.* [18,19] note the limitations of the collinear approximation in the treatment of temperature-induced interatomic forces. The constrained method offers a way forward in the *ab initio* treatment of noncollinear magnetic excitations essential for the first-principles analysis of finite temperature effects in magnetic materials.

B. Fe_2 dimer

In this section we investigate a Fe_2 dimer. Calculations are performed for two Fe atoms placed in a rectangular box with dimensions 10 Å × 10 Å × 10 Å, with k-point sampling reduced to a single Γ point. While constraining the angle between magnetic moments of the two atoms, we allow full relaxation of the bond length R_b. The results are compared with energies computed for collinear ferromagnetic and antiferromagnetic configurations. The difference between the energies found using a nonconstrained conventional DFT functional, and the new constrained functional, is found to be less than 0.1 meV.

Figure 9(a) shows the binding energy E_B plotted as a function of the angle between magnetic moments. E_B is maximum for the ferromagnetic state, where $E_B = 3.02$ eV. E_B then decreases as a function of the angle and reaches minimum at 180°. The antiferromagnetic state of a Fe_2 molecule is metastable. The binding energy in the antiferromagnetic state is $E_B = 1.59$ eV. The difference between the energies of ferromagnetic and antiferromagnetic states is 1.43 eV, and the energy landscape is fairly flat in the vicinity of 0 and 180 degree points.

Figure 9(b) shows the calculated equilibrium bond length R_b plotted as a function of the angle between the two moments. In the ferromagnetic state the value of R_b is the lowest, and is equal to 2.03 Å. It is maximum at approximately 160°, where it approaches 2.29 Å, and then it decreases to 2.25 Å in the antiferromagnetic configuration where the angle between the moments equals 180°.

Figure 9(c) shows atomic magnetic moment $|\mathbf{M}_I|$ calculated by projecting the magnetization density onto a sphere with radius $R = 1.0$ Å. At the point where magnetic moments are ferromagnetically ordered (this corresponds to 0°) $|\mathbf{M}_I| = 2.796\mu_B$. The moments then decrease gradually, reaching maximum at approximately 160°, and then decrease again. In the antiferromagnetic state, $|\mathbf{M}_I| = 2.753\mu_B$. The scale of variation of moments is relatively small, of the order of $0.1\mu_B$. Far more substantial variation is observed in bulk bcc iron, as shown in Fig. 6. Since the bond length decreases when the angle exceeds 160°, whereas the binding energy remains almost constant, this appears to be the result of interplay between bonding and charge density distributions. This interpretation agrees with the fact that magnetic moment magnitude also changes its slope near 160°.

Using rare gas matrix isolation and extended x-ray absorption fine structures (EXAFS) technique, R_b of a Fe_2 dimer in argon [66] was measured experimentally to be 1.87 ± 0.13 Å, and in neon [67] it is 2.02 ± 0.02 Å, where the latter value should be considered as corresponding to a mixture of multimers. Using collision-induced dissociation, E_B is determined to be [68] 1.14 ± 0.10 eV. Using the Stern-Gerlach deflection method, the total magnetic moment of a dimer was found to be [69] $6.5 \pm 1\mu_B$.

Magnetic and electronic structures of a Fe_2 dimer were extensively studied in literature. Chen *et al.* [70] used an all-electron linear combination of atomic orbitals (LCAO) method in the local spin density approximation (LSDA) and found equilibrium bond length $R_b = 1.98$ Å, $E_B =$

TABLE I. The calculated and experimental values of the binding energy E_B, bond length R_b, and magnetic moment of an atom $|\mathbf{M}_I|$ in a Fe_2 dimer.

Authors	DFT functional / Expt. method	State	E_B (eV)	R_b (Å)	$\lvert\mathbf{M}_I\rvert$ (μ_B)
Current work	GGA-PBE [63]	FM	3.02	2.03	2.796
		AFM	1.59	2.25	2.753
Chen *et al.* [70]	LSDA	FM	4.095	1.98	3
		AFM	1.95	2.20	4.8
Diéguez *et al.* [71]	LSDA	FM	4.5	1.96	3
Castro *et al.* [72,73]	LSDA	FM	4.38	1.95	–
	GGA-P86 [74]	FM	3.24	2.00	–
	GGA-P86 (Non-spherical)	FM	2.08	–	–
Hobbs *et al.* [25]	GGA-P92 [75]	FM	3.54	1.98	2.83
		AFM	2.246	2.24	2.98
Lian *et al.* [68]	Expt. - Collision-induced dissociation	?	1.14 ± 0.10	–	–
Montano *et al.* [66]	Expt. - EXAFS (argon)	?	–	1.87 ± 0.13	–
Purdum *et al.* [67]	Expt. - EXAFS (neon)	?	–	2.02 ± 0.02	-
Cox *et al.* [69]	Expt. - Stern-Gerlach deflection	?	–	–	3.25 ± 0.5

4.095 eV, and $|\mathbf{M}_I| = 3\mu_B$/atom in the ferromagnetic, and $R_b = 2.20$ Å, $E_B = 1.95$ eV, and $|\mathbf{M}_I| = 4.8\mu_B$/atom in the antiferromagnetic configuration. Diéguez *et al.* [71] used LSDA and eight valence electrons, and found $R_b = 1.96$ Å, $E_B = 4.5$ eV, $|\mathbf{M}_I| = 3\mu_B$/atom in the ferromagnetic ground state of the molecule. Castro *et al.* [72,73] used an all-electron linear combination of Gaussian-type orbitals, and LSDA, GGA-P86 [74], and GGA-P86 functional with nonspherical (NS) charge density. In LSDA, the predicted bond length and the binding energy are $R_b = 1.95$ Å and $E_B = 4.38$ eV. Using GGA-P86 they found $R_b = 2.00$ Å and $E_B = 3.24$ eV. In the GGA-NS the binding energy is relatively small $E_B = 2.08$ eV. Hobbs *et al.* [25] found $R_b = 1.98$ Å, $E_B = 3.54$ eV, and $|\mathbf{M}_I| = 2.83\mu_B$/atom in the ferromagnetic state, and $R_b = 2.24$ Å, $E_B = 2.246$ eV, and $|\mathbf{M}_I| = 2.98\mu_B$/atom in the antiferromagnetic state. The latter calculations were performed using the GGA-P92 [75] functional, with the plane wave energy cutoff of 350 eV, and $R = 1.2$ Å. We listed those experimental and calculated results in Table I.

While the absolute values of energies predicted by DFT for molecules are known to be of limited validity, the above analysis confirms that calculations performed using the new constrained functional methodology compare well with literature data on ferromagnetic and antiferromagnetic states. The scatter of results is largely due to the choice of exchange correlation functionals. Here we used the same GGA-PBE functional as in the rest of the paper, where we apply it to the treatment of high-density atomic configurations where DFT methodology is known to have high predictive capability.

C. Amorphous Fe

An atomic configuration of amorphous Fe containing 54 atoms in a unit cell was derived from molecular dynamic (MD) simulations performed using the Dudarev-Derlet interatomic potential [76]. A 54-atom bcc Fe cell was heated up dynamically to 10 000 K and then relaxed using conjugate gradient minimization. The resulting atomic configurations were used as input for VASP calculations, performed using GGA-PBE and a $4 \times 4 \times 4$ k-point mesh. Other parameters are the same as in calculations described above. Ionic relaxation is performed in the unconstrained collinear approximation until the interatomic forces decrease below 0.01 eV/Å. Magnetic moments are evaluated by projecting the magnetization density onto spheres with radius $R = 1.0$ Å.

Figure 10(a) shows a fully relaxed atomic and magnetic configuration derived from an unconstrained collinear magnetic calculation. The magnitude of forces acting on atoms is smaller than 0.01 eV/Å. This example shows that directions and magnitudes of magnetic moments fluctuate strongly depending on the local atomic environment. The magnitude of $|\mathbf{M}_I|$ varies from $0.034\mu_B$ to $2.59\mu_B$.

We now generate a random magnetic configuration and impose it onto the *atomic* configuration shown in Fig. 10(a) through the application of the constrained method. Figure 10(b) shows directions and magnitudes of magnetic moments in the resulting magnetic structure. The magnitudes of magnetic moments $|\mathbf{M}_I|$ vary from $0.86\mu_B$ to $2.46\mu_B$, showing that magnetic moment magnitudes are highly sensitive to the local *magnetic* environment, since in constrained

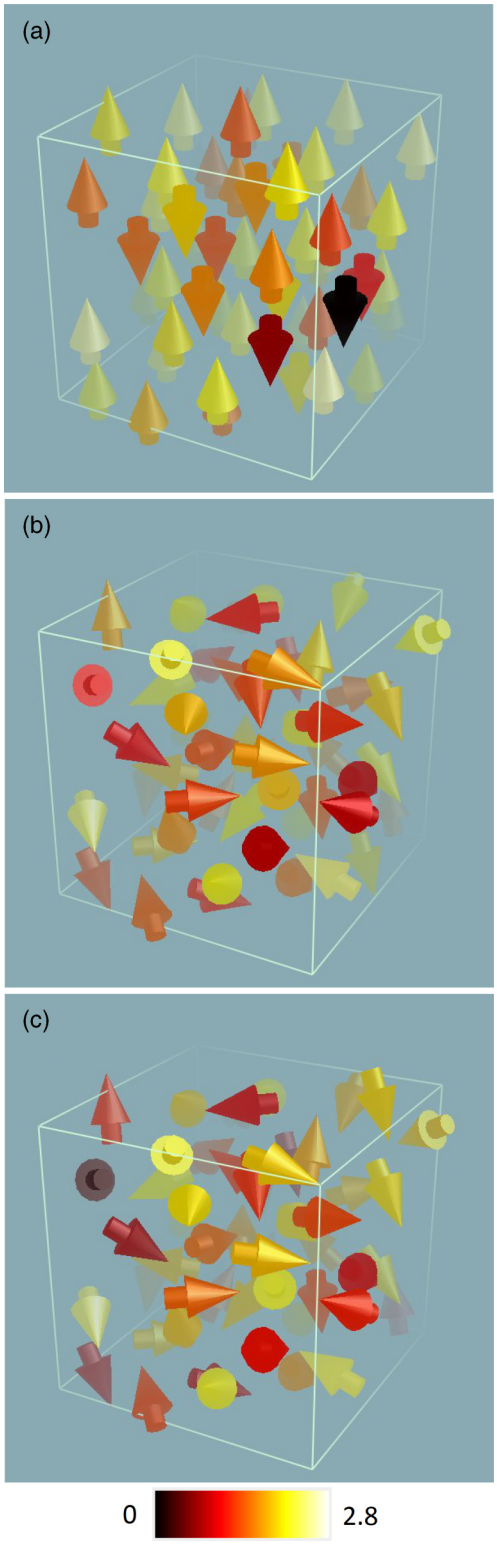

FIG. 10. (Color online) Directions and magnitudes of magnetic moments in amorphous Fe. (a) Unconstrained collinear configuration computed using full ionic relaxation. (b) Constrained noncollinear calculation with random orientations of magnetic moments, generated using atomic positions derived from the unconstrained collinear calculation. (c) Constrained noncollinear calculation with the same magnetic moments as in (b) but with full ionic relaxation. Colors refer to the magnitude of atomic magnetic moments.

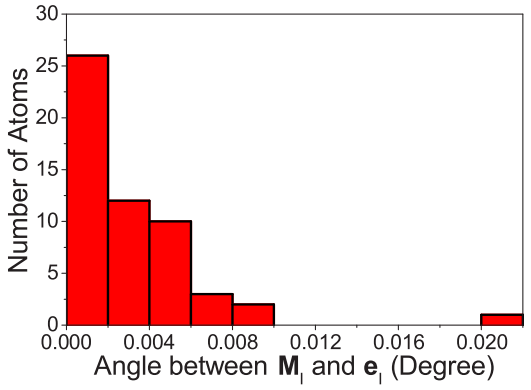

FIG. 11. (Color online) Histogram distribution of angles between the local magnetic moments $\mathbf{M}_I$ and their directions $\mathbf{e}_I$ defined in the constraining functional, evaluated for the configuration shown in Fig. 10(c).

calculations the positions of atoms remain constant. The energies of configurations shown in Fig. 10(b) are 2.98 eV higher than the energies of collinear configuration shown in Fig. 10(a).

To investigate the effect of magnetism on atomic positions we now relax the atomic coordinates, keeping the same *directions* of magnetic moments as in Fig. 10(b). Atomic relaxation is performed until the forces acting on atoms, shown in Fig. 10(c), become smaller than 0.01 eV/Å. The magnitude of $|\mathbf{M}_I|$ in the resulting atomically relaxed configuration spans the interval from $0.22\mu_B$ to $2.42\mu_B$. The energy of configuration shown in Fig. 10(c) is 0.75 eV lower than the energy of configuration shown in Fig. 10(b), showing that atomic and directional magnetic degrees of freedom are fundamentally linked, with forces acting on atoms being sensitive to the directions of magnetic moments and atomic relaxations affecting the magnitudes of local magnetic moments.

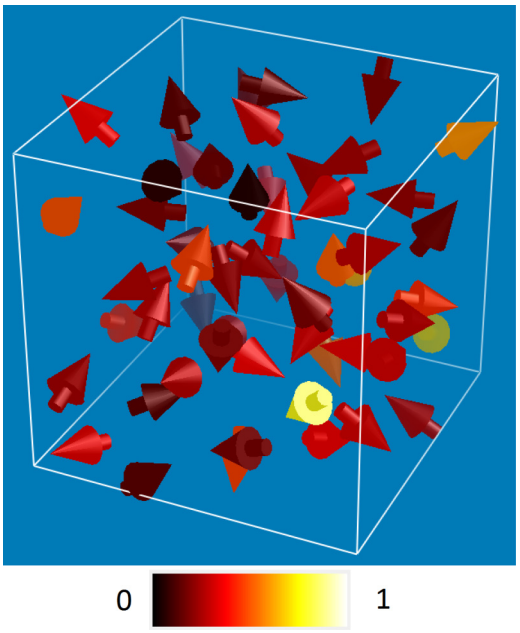

FIG. 12. (Color online) Interatomic forces resulting from the noncollinearity of local magnetic moments. The atomic configuration is the same as in Fig. 10(b), with colors showing magnitudes of forces acting on atoms, in eV/Å units.

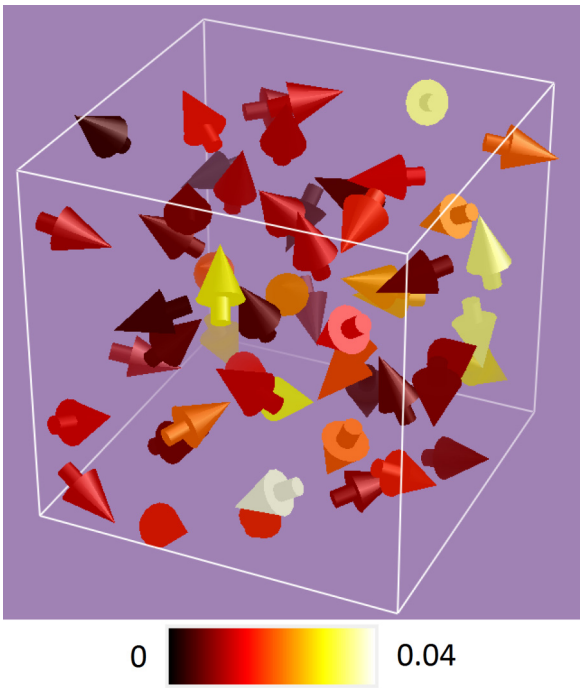

FIG. 13. (Color online) Atomic displacements corresponding to the difference between atomic positions in configurations shown in Figs. 10(b) and 10(c). Colors denote the magnitude of atomic displacements, in Å units.

In Fig. 11 we show a histogram of angles between the local magnetic moments $\mathbf{M}_I$ and their directions $\mathbf{e}_I$ prescribed in the constrained functional, computed for the configuration shown in Fig. 10(c). The values deviate by no more than 0.02°, confirming that the constrained functional can be applied to arbitrary atomic and magnetic configurations.

Figure 12 shows atomic forces in the configuration shown in Fig. 10(b). The maximum force on an atom is 0.77 eV/Å. In agreement with the case of a diatomic molecule, we find that magnetic excitations induce forces and modify equilibrium atomic configurations. To quantify this, in Fig. 13 we show atomic displacements corresponding to configurations shown in Figs. 10(b) and 10(c). The maximum displacement of atoms from their initial position is approximately 0.039 Å.

We therefore conclude that directional degrees of freedom of magnetic moments affect interatomic forces and equilibrium atomic positions. Practical calculations required for quantifying the effect of directional magnetic excitations on atomic forces and positions of atoms, for even fairly complex atomic configurations, can be performed using the constrained density functional method with appropriately chosen Lagrange multipliers, as illustrated by the examples given above.

V. CONCLUSIONS

In this paper we develop the formalism and give examples of application of a constrained density functional method for generating noncollinear magnetic configurations. We show

that the method exhibits good convergence and is fairly easy to implement. Using VASP platform for its implementation, we explored the effect of magnetic noncollinearity on atomic configurations of iron. The main advantage of the method is that it makes it possible to explore magnetic configurations where magnetic moments point in arbitrary directions, like in realistic thermal excitations, whereas the majority of calculations described in literature focus solely on collinear ferromagnetic and antiferromagnetic states. For the collinear configurations, the energies and atomic configurations predicted using the constrained method agree well with published data. For the noncollinear configurations, we are able to quantitatively assess the effect of magnetic noncollinearity on interatomic forces and equilibrium atomic positions.

ACKNOWLEDGMENTS

This work was partly funded by the RCUK Energy Programme (Grant No. EP/I501045), and has been carried out within the framework of the EUROfusion Consortium and has received funding from the Euratom research and training program 2014-2018 under Grant Agreement No. 633053. To obtain further information on the data and models underlying this paper please contact PublicationsManager@ccfe.ac.uk. The views and opinions expressed herein do not necessarily reflect those of the European Commission. This work was also partly funded by the United Kingdom Engineering and Physical Sciences Research Council via Grant No. EP/G050031. The authors would like to thank Duc Nguyen-Mahn, Jan Wróbel, Fritz Körmann, and Jorg Neugebauer for stimulating discussions.

APPENDIX: VASP IMPLEMENTATION

There are two constrained approaches to the treatment of noncollinear magnetic configurations presently implemented in VASP. The first constrains atomic magnetic moments to prescribed directions but is invariant with respect to the reversal of directions of moments. The second method exhibits good convergence in the limit of large λ. However, since no convergence analysis is available in the literature, we present such analysis here.

The constrained total energy functional described above has the form,

$$E = E_0 + E_p \tag{A1}$$

$$= E_0 + \sum_I \lambda(\Delta\mathbf{M}_I)^2, \tag{A2}$$

where $\Delta\mathbf{M}_I = \mathbf{M}_I - \mathbf{M}_I^0$ and $\mathbf{M}_I^0$ is the desired magnetic moment vector. At an extremum, for example, in the magnetic ground state of the system, the derivative of the total energy with respect to any $\Delta\mathbf{M}_I$ must vanish, namely

$$0 = \left.\frac{\delta E}{\delta \mathbf{M}_I}\right|_{\Delta\mathbf{M}_I} = \left.\frac{\delta E_0}{\delta \mathbf{M}_I}\right|_{\Delta\mathbf{M}_I} + 2\lambda\Delta\mathbf{M}_I. \tag{A3}$$

Hence

$$\Delta\mathbf{M}_I = -\frac{1}{2\lambda}\left.\frac{\delta E_0}{\delta \mathbf{M}_I}\right|_{\Delta\mathbf{M}_I}. \tag{A4}$$

For small $\Delta\mathbf{M}_I$ we perform Taylor expansion up to the first order in the right-hand side, and find that

$$\Delta\mathbf{M}_I = -\frac{1}{2\lambda}(\mathbf{K}_1 + \underline{K}_2 \cdot \Delta\mathbf{M}_I), \tag{A5}$$

where

$$\mathbf{K}_1 = \left.\frac{\delta E_0}{\delta \mathbf{M}_I}\right|_0, \tag{A6}$$

$$\underline{K}_2 = \left.\frac{\delta^2 E_0}{\delta \mathbf{M}_I^2}\right|_0. \tag{A7}$$

Here $\underline{K}_2$ is a 3×3 matrix. After rearranging the terms, we arrive at

$$\Delta\mathbf{M}_I = -\frac{1}{2\lambda}\left(\underline{I} + \frac{1}{2\lambda}\underline{K}_2\right)^{-1} \cdot \mathbf{K}_1, \tag{A8}$$

where $\underline{I}$ is a 3×3 identity matrix. We see that $\Delta\mathbf{M}_I \propto 1/\lambda$ in the limit where λ is large. Hence we conclude that $E_p \propto 1/\lambda$ and in the limit where $\lambda \to \infty$ we have $E_p \to 0$.

[1] M. Yu. Lavrentiev, R. Soulairol, C.-C. Fu, D. Nguyen-Manh, and S. L. Dudarev, Phys. Rev. B **84**, 144203 (2011).
[2] J. E. Peralta, G. E. Scuseria, and M. J. Frisch, Phys. Rev. B **75**, 125119 (2007).
[3] J. Sticht, K.-H. Höck, and J. Kübler, J. Phys. Condens. Matter **1**, 8155 (1989).
[4] Y. Kakehashi and T. Uchida, J. Phys. Condens. Matter **12**, 8683 (2000).
[5] N. N. Delyagin, A. L. Erzinkyan, V. P. Parfenova, and I. N. Rozantsev, J. Mag. Mag. Mater. **323**, 3058 (2011).
[6] L. Gondek, A. Szytula, S. Baran, and J. Hernandez-Velasco, J. Mag. Mag. Mater. **272**, E443 (2004).
[7] Y. Tsunoda, J. Phys. Condens. Matter **1**, 10427 (1989).
[8] O. N. Mryasov, V. A. Gubanov, and A. I. Liechtenstein, Phys. Rev. B **45**, 12330 (1992).
[9] M. Körling and J. Ergon, Phys. Rev. B **54**, R8293 (1996).
[10] K. Knöpfle, L. M. Sandratskii, and J. Kubler, Phys. Rev. B **62**, 5564 (2000).
[11] O. N. Mryasov, A. I. Lichtenstein, L. M. Sandratskii, and V. A. Gubanov, J. Phys. Condens. Matter **3**, 7683 (1991).
[12] D. M. Bylander and L. Kleinman, Phys. Rev. B **58**, 9207 (1998).
[13] E. Sjöstedt and L. Nordström, Phys. Rev. B **66**, 014447 (2002).
[14] P.-W. Ma, C. H. Woo, and S. L. Dudarev, Phys. Rev. B **78**, 024434 (2008).
[15] P.-W. Ma, C. H. Woo, and S. L. Dudarev, Phil. Mag. **89**, 2921 (2009).
[16] P.-W. Ma and S. L. Dudarev, Phys. Rev. B **86**, 054416 (2012).
[17] A. V. Ruban and V. I. Razumovskiy, Phys. Rev. B **85**, 174407 (2012).
[18] F. Körmann, A. Dick, B. Grabowski, T. Hickel, and J. Neugebauer, Phys. Rev. B **85**, 125104 (2012).

[19] F. Körmann, B. Grabowski, B. Dutta, T. Hickel, L. Mauger, B. Fultz, and J. Neugebauer, Phys. Rev. Lett. **113**, 165503 (2014).
[20] U. von Barth and L. Hedin, J. Phys. C **5**, 1629 (1972).
[21] L. Sandratskii and P. Guletskii, J. Phys. F: Met. Phys. **16**, L43 (1986).
[22] J. Kübler, K. Höck, J. Sticht, and A. Williams, J. Phys. F: Met. Phys. **18**, 469 (1988).
[23] L. Nordström and D. J. Singh, Phys. Rev. Lett. **76**, 4420 (1996).
[24] T. Oda, A. Pasquarello, and R. Car, Phys. Rev. Lett. **80**, 3622 (1998).
[25] D. Hobbs, G. Kresse, and J. Hafner, Phys. Rev. B **62**, 11556 (2000).
[26] K. Nakamura, T. Ito, A. J. Freeman, L. Zhong, and J. Fernandez-de-Castro, Phys. Rev. B **67**, 014420 (2003).
[27] Ph. Kurz, F. Förster, L. Nordström, G. Bihlmayer, and S. Blügel, Phys. Rev. B **69**, 024415 (2004).
[28] R. Singer, M. Fähnle, and G. Bihlmayer, Phys. Rev. B **71**, 214435 (2005).
[29] http://www.quantum-espresso.org/.
[30] http://www.openmx-square.org/.
[31] G. Kresse and J. Hafner, Phys. Rev. B **47**, 558(R) (1993); **49**, 14251 (1994); G. Kresse and J. Furthmuller, Comput. Mat. Sci. **6**, 15 (1996); Phys. Rev. B **54**, 11169 (1996).
[32] C. Domain and C. S. Becquart, Phys. Rev. B **65**, 024103 (2001).
[33] C.-C. Fu, F. Willaime, and P. Ordejón, Phys. Rev. Lett. **92**, 175503 (2004).
[34] D. Nguyen-Manh, A. P. Horsfield, and S. L. Dudarev, Phys. Rev. B **73**, 020101(R) (2006).
[35] S. L. Dudarev, R. Bullough, and P. M. Derlet, Phys. Rev. Lett. **100**, 135503 (2008).
[36] H. C. Herper, E. Hoffmann, and P. Entel, Phys. Rev. B **60**, 3839 (1999).
[37] R. Soulairol, C.-C. Fu, and C. Barreteau, J. Phys. Condens. Matter **22**, 295502 (2010).
[38] M. Y. Lavrentiev, D. Nguyen-Manh, and S. L. Dudarev, Phys. Rev. B **81**, 184202 (2010).
[39] D. Nguyen-Manh, M. Y. Lavrentiev, M. Muzyk, and S. L. Dudarev, J. Mater. Sci. **47**, 7385 (2012).
[40] S. L. Dudarev, Annu. Rev. Mater. Res. **43**, 35 (2013).
[41] M. Y. Lavrentiev, J. S. Wróbel, D. Nguyen-Manh, and S. L. Dudarev, Phys. Chem. Chem. Phys. **16**, 16049 (2014).
[42] V. I. Razumovskiy, A. V. Ruban, and P. A. Korzhavyi, Phys. Rev. Lett. **107**, 205504 (2011).
[43] A. V. Ruban, P. A. Korzhavyi, and B. Johansson, Phys. Rev. B **77**, 094436 (2008).
[44] T. P. C. Klaver, R. Drautz, and M. W. Finnis, Phys. Rev. B **74**, 094435 (2006).
[45] A. T. Paxton and M. W. Finnis, Phys. Rev. B **77**, 024428 (2008).
[46] P. Olsson, T. P. C. Klaver, and C. Domain, Phys. Rev. B **81**, 054102 (2010).
[47] H. Wen, P.-W. Ma, and C. H. Woo, J. Nucl. Mater. **440**, 428 (2013).
[48] H. Wen and C. H. Woo, J. Nucl. Mater. **455**, 31 (2014).
[49] V. P. Antropov, M. I. Katsnelson, M. van Schilfgaarde, and B. N. Harmon, Phys. Rev. Lett. **75**, 729 (1995).
[50] V. P. Antropov, M. I. Katsnelson, B. N. Harmon, M. van Schilfgaarde, and D. Kusnezov, Phys. Rev. B **54**, 1019 (1996).
[51] O. Ivanov and V. Antropov, J. Appl. Phys. **85**, 4821 (1999).
[52] M. Fähnle, R. Drautz, R. Singer, D. Steiauf, and D. V. Berkov, Comp. Mater. Sci. **32**, 118 (2005).
[53] B. Újfalussy, X.-D. Wang, D. M. C. Nicholson, W. A. Shelton, G. M. Stocks, Y. Wang, and B. L. Györffy, J. Appl. Phys. **85**, 4824 (1999).
[54] G. M. Stocks, B. Újfalussy, X.-D. Wang, D. M. C. Nicholson, W. A. Shelton, Y. Wang, A. Canning, and B. L. Györffy, Philso. Mag. B **78**, 665 (1998).
[55] P. H. Dederichs, S. Blügel, R. Zeller, and H. Akai, Phys. Rev. Lett. **53**, 2512 (1984).
[56] B. Kaduk, T. Kowalczyk, and T. van Voorhis, Chem. Rev. **112**, 321 (2012).
[57] H. Köhler, J. Sticht, and J. Kübler, Physica B **172**, 79 (1991).
[58] S. Morán, C. Ederer, and M. Fähnle, Phys. Rev. B **67**, 012407 (2003).
[59] M. Ležaić, P. Mavropoulos, G. Bihlmayer, and S. Blügel, Phys. Rev. B **88**, 134403 (2013).
[60] P. E. Blochl, Phys. Rev. B **50**, 17953 (1994); G. Kresse and D. Joubert, *ibid.* **59**, 1758 (1999).
[61] R. F. W. Bader, *Atoms in Molecules – A Quantum Theory* (Oxford University Press, Oxford, 1990).
[62] W. Tang, E. Sanville, and G. Henkelman, J. Phys.: Condens. Matter **21**, 084204 (2009); E. Sanville, S. D. Kenny, R. Smith, and G. Henkelman, J. Comp. Chem. **28**, 899 (2007); G. Henkelman, A. Arnaldsson, and H. Jónsson, Comput. Mater. Sci. **36**, 354 (2006).
[63] J. P. Perdew, K. Burke, and M. Ernzerhof, Phys. Rev. Lett. **77**, 3865 (1996).
[64] L. Schimka, R. Gaudoin, J. Klimeš, M. Marsman, and G. Kresse, Phys. Rev. B **87**, 214102 (2013).
[65] J. S. Wróbel, D. Nguyen-Manh, M. Yu. Lavrentiev, M. Muzyk, and S. L. Dudarev, Phys. Rev. B **91**, 024108 (2015).
[66] P. A. Montano and G. K. Shenoy, Solid State Commun. **35**, 53 (1980).
[67] H. Purdum, P. A. Montano, G. K. Shenoy, and T. Morrison, Phys. Rev. B **25**, 4412 (1982).
[68] L. Lian, C.-X. Su, and P. B. Armentrout, J. Chem. Phys. **97**, 4072 (1992).
[69] D. M. Cox, D. J. Trevor, R. L. Whetten, E. A. Rohlfing, and A. Kaldor, Phys. Rev. B **32**, 7290 (1985).
[70] J. L. Chen, C. S. Wang, K. A. Jackson, and M. R. Pederson, Phys. Rev. B **44**, 6558 (1991).
[71] O. Diéguez, M. M. G. Alemany, C. Rey, P. Ordejón, and L. J. Gallego, Phys. Rev. B **63**, 205407 (2001).
[72] M. Castro and D. R. Salahub, Phys. Rev. B **49**, 11842 (1994).
[73] M. Castro, C. Jamorski, and D. R. Salahub, Chem. Phys. Lett. **271**, 133 (1997).
[74] J. P. Perdew and Y. Wang, Phys. Rev. B **33**, 8800 (1986); J. P. Perdew, *ibid.* **33**, 8822 (1986); **34**, 7406 (1986).
[75] J. P. Perdew, J. A. Chevary, S. H. Vosko, K. A. Jackson, M. R. Pederson, D. J. Singh, and C. Fiolhais, Phys. Rev. B **46**, 6671 (1992); **48**, 4978 (1993).
[76] S. L. Dudarev and P. M. Derlet, J. Phys. Condens. Matter **17**, 7097 (2005).